Supporting Information

Rare Earth Orthovanadates (REM-VO_4; REM= Pr, Gd, & Sm)-based Sensor for Selective and Simultaneous Detection of Furazolidone and Metronidazole

Pandiyan Bharathi, Sea-Fue Wang[*]

Department of Materials and Mineral Resources Engineering, National Taipei University of Technology, Taipei 106, Taiwan.

[*]**Corresponding author:**

S.-F. Wang, Email: sfwang@ntut.edu.tw

1. Materials characterizations

The phase analysis, functional group analysis, and the material's oxidation states are analyzed by X-ray diffraction analysis (XRD) (Brucker, Rigaku D/maxB, DMX-2200), Fourier-transform infrared spectrometry (FT-IR) (Model: Jasco FT-IR- 4600), Raman spectroscopy (Model: Thermo ESCLB 250), and X-ray photoelectron spectroscopy (XPS) ESCA/Auger Laboratory respectively. The morphological and elemental analysis was done by transmission electron microscope (TEM) (JEOL JEM-2100F (HR)) operating at 200 kV and energy-dispersive X-ray spectroscopy using EDAX AMETEK Inc., the Digital Micrograph® software.

2. Electrochemical measurements

The electrochemical impedance spectroscopy was performed in Autolab (PGSTAT101) in the frequency range of 100 kHz-0.1 Hz. All the other electrochemical studies including cyclic voltammetry (CV) and differential pulse voltammetry (DPV) are done by CHI 1211c electrochemical workstation. A standard three-electrode system: working electrode (Glassy carbon electrode (GCE)), reference electrode (Ag/AgCl), and counter electrode (Pt wire) were used as an electrochemical probe. The applied potential window for the EASA and FD & MD detection was performed between -0.2 V to 0.6V. The additional parameters are Electrolyte mediums (5 mM of $[Fe(CN)_6]^{3-/4-}$ for EASA and EIS analysis, 0.1 M PBS for FD & MD detection; sensitivity ($1.e^{-005}$) and scan rate (50 mV/s).

Table S1. The Raman modes of REM-VO_4 (REM- Pr, Gd & Sm).

Raman shift (cm^{-1})			**Symmetry**	**Assignment**
$PrVO_4$	**$GdVO_4$**	**$SmVO_4$**		
902.6	902.6	900.4	A_{1g}	VO_4^{3-} symmetry vibration
837.6	839.7	837.6	E_g	asymmetry vibration
160.7	153.7	158.4	E_g	external mode of vibration
302.3	297.8	300.1	B_{2g}	
421.4	421.5	419.2	B_{2g}	

Table S2. XPS analysis of REM-VO_4 (REM- Pr, Gd & Sm).

Materials	**Element**		**Binding energy (eV)**
$PrVO_4$	Pr	Pr^{4+} $3d_{5/2}$	≈ 927.1
		Pr^{4+} $3d_{3/2}$	≈ 947.6
		Pr^{3+} $3d_{5/2}$	≈ 923.2
		Pr^{3+} $3d_{3/2}$	≈942.9
	V	V^{5+} $2p_{3/2}$	≈ 517.6
		V^{5+} $2p_{1/2}$	≈ 525.0
	O	M-O	≈ 530.2
		Absorbed H_2O	≈ 532.9
$GdVO_4$	Gd	$3d_{5/2}$	≈ 1187.3
		$3d_{3/2}$	≈ 1219.3
	V	V^{5+} $2p_{3/2}$	≈ 516.4
		V^{5+} $2p_{1/2}$	≈ 523.8
	O	M-O	≈ 529.5
		Absorbed H_2O	≈ 531.5
$SmVO_4$	Sm	$3d_{5/2}$	≈ 1080.1
		$3d_{3/2}$	≈ 1107. 8
	V	V^{5+} $2p_{3/2}$	≈ 516.1
		V^{5+} $2p_{1/2}$	≈ 522.9
	O	M-O	≈ 529.2
		Absorbed H_2O	530.4

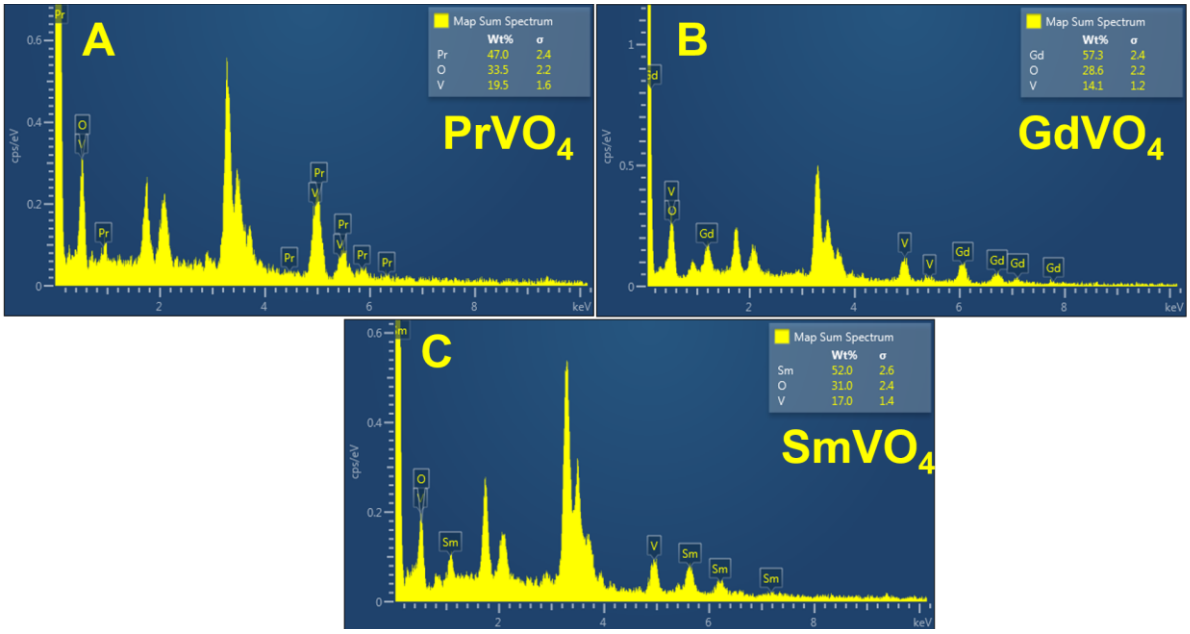

Figure S1. EDX spectra of (A) $PrVO_4$, (B) $GdVO_4$, and (C) $SmVO_4$

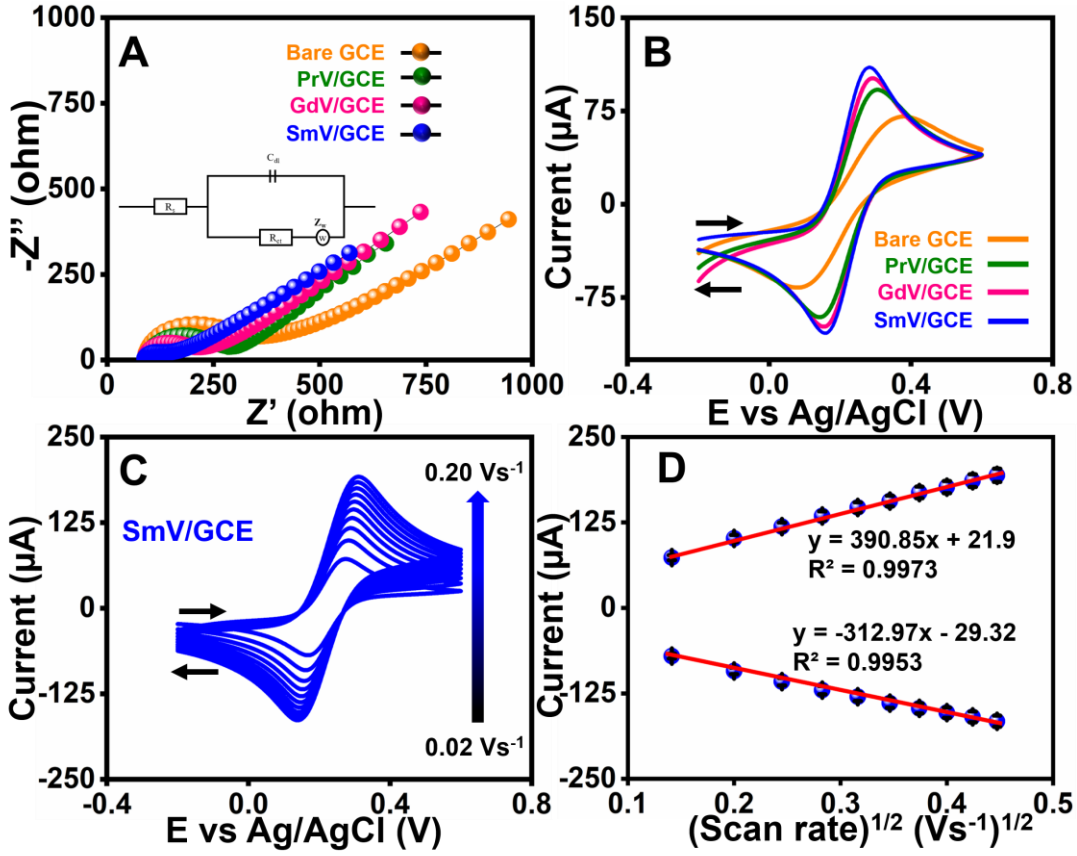

Figure S2. (A) EIS (Inset: Randles circuit model), (B) CV of modified electrodes, (C) CV profiles of SmV/GCE at different scan rates, (D) corresponding linear plot

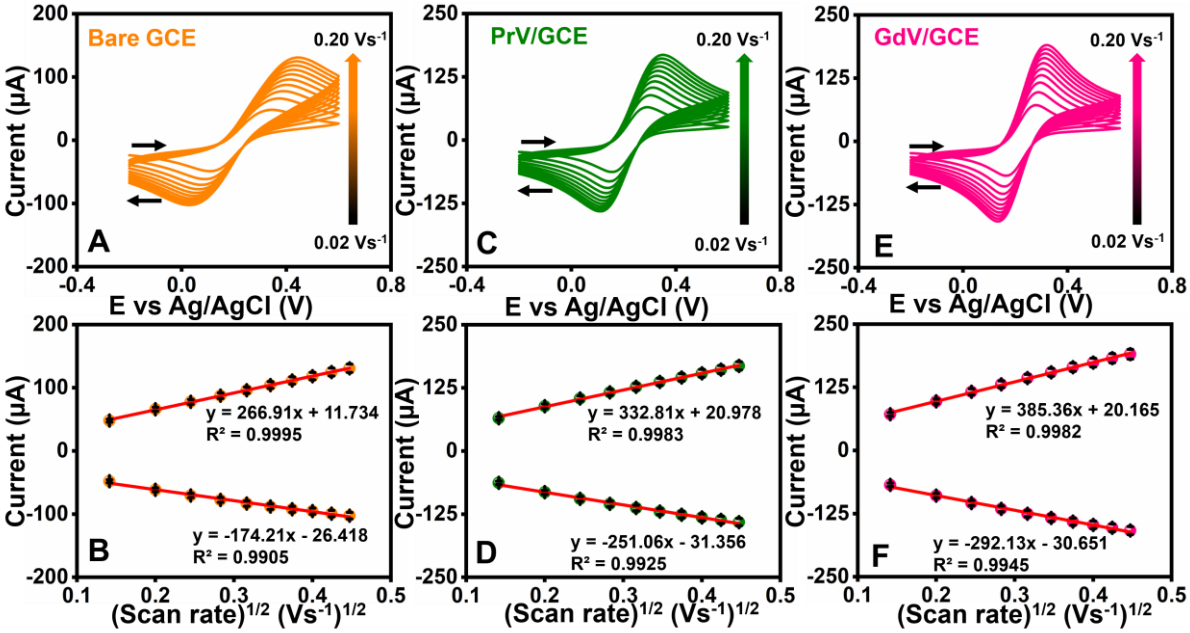

Figure S3. CV profiles of (A) Bare GCE, (C) PrV/GCE, (E) GmV/GCE at different scan rates, and (B, D & F) respective linear plots.

Table S3. The EIS parameters of REM-VO_4(REM- Pr, Gd & Sm)

Modified electrodes	R_s (Ω·cm^2)	R_{ct} (Ω·cm^2)	ESR (Ω·cm^2)	K_s
Bare-GCE	88.0	278.6	366.6	1.60E^{-08}
PrV/GCE	90.1	205.1	295.2	2.18E^{-08}
GdV/GCE	88.2	130.0	218.3	3.43E^{-08}
SmV/GCE	87.7	56.8	144.5	7.86E^{-08}

Table S4. The CV parameters of REM-V/GCE (REM- Pr, Gd & Sm) in the presence of FD and MD.

Modified electrodes	Individual detection				Simultaneous detection			
	FD		MD		FD		MD	
	I_{pa} (µA)	E_{pa} (V)	I_{pa} (µA)	E_{pa} (V)	I_{pa} (µA)	E_{pa} (V)	I_{pa} (µA)	E_{pa} (V)
Bare-GCE	-9.07	-0.41	-10.10	-0.64	-9.18	-0.39	-10.31	-0.64
PrV/GCE	-11.98	-0.39	-12.58	-0.63	-11.89	-0.40	-13.18	-0.66
GdV/GCE	-14.30	-0.38	-13.88	-0.63	-14.73	-0.39	-15.48	-0.63
SmV/GCE	-16.28	-0.40	-15.35	-0.64	-17.07	-0.38	-16.19	-0.62

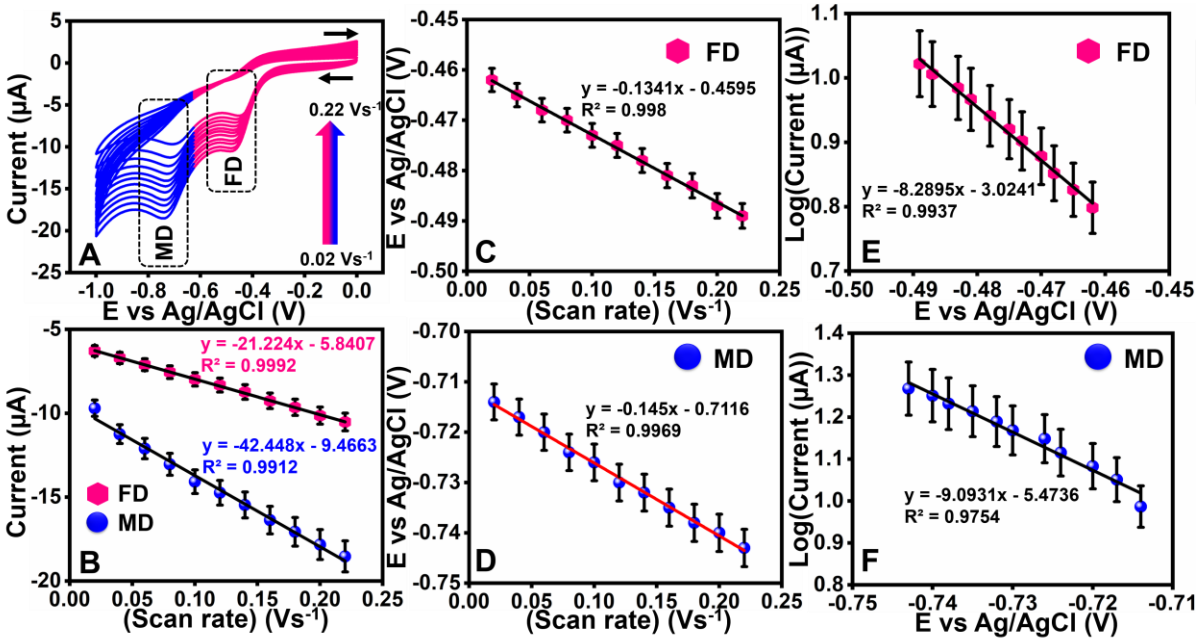

Figure S4. (A) CV response of SmV/GCE at different scan rates (B) linear plot of scan rate vs. current (FD & MD), (C) linear plot of scan rate vs. peak potential (FD), (D) linear plot of scan rate vs. peak potential (MD), (E) linear plot of peak potential vs. log of current (FD), and (F) linear plot of peak potential rate vs. log of current (MD).

Table S5. The LOD and linear range (LR) of REM-V/GCE (REM- Pr, Gd & Sm) in the presence of FD and MD.

Modified electrodes	Individual detection				Simultaneous detection			
	FD		MD		FD		MD	
	LOD (μM)	LR (μM)	LOD (μM)	LR (μM)	LOD (μM)	LR (μM)	LOD (μM)	LR (μM)
Bare-GCE	0.5245	0.1 - 161.0	0.9302	0.1 - 161.0	0.7782	0.5 - 383.5	1.1106	0.5 - 383.5
PrV/GCE	0.0125		0.0361		0.0191		0.0465	
GdV/GCE	0.0089		0.0160		0.0116		0.0201	
SmV/GCE	0.0009		0.0036		0.0015		0.0049	

Table S6. Comparison table of FD determination.

Materials	**Linear range (μM)**	**Limit of detection (μM))**	**pH**	**Detection technique**	**Ref.**
RGO	0.001-10.0	0.003	7.4	LSV	1
MWCNT	3.0-800.0	0.0023	6.8	DPV	2
Gr/Au	1.0-674.0	0.064	6.0	i-t	3
MoO_3/g-C_3N_4	0.01-228	0.0014	7.0	i-t	4
h-BN/HNTs	0.009-173.0	0.001	7.0	i-t	5
Pt-Re NP/PAC	0.2-117.7	0.0208	7.0	DPV	6
Pt-Re NP/PAC	1.0-299	0.0755	7.0	LSV	6
SnS_2-SnO_2/graphene	0.015-190.5	0.0014	7.0	DPV	7
COF@NH_2-CNT	0.2-100	0.0775	7.0	DPV	8
$NiFe_2O_4$/rGO	0.1-150	0.050	7.0	DPV	9
MIP-MWCNTs	0.01-1	0.030	7.0	DPV	10
$SmVO_4$	**0.1-161.0**	**0.0009**	**7.0**	**DPV**	**This work**

RGO- reduced graphene oxide; MWCNT-multi-walled carbon nanotube; Gr/Au-graphene/gold nanoparticles; MoO_3/g-C_3N_4- molybdenum oxide/graphitic carbon nitride; h-BN/HNTs- hexagonal boron nitride/halloysite nanotubes; Pt-Re NP/PAC- platinum-rhenium nanoparticles/porous activated carbon; SnS_2-SnO_2/graphene- tin sulfide-tin oxide/graphene; COF@NH_2-CNT- covalent organic framework@amino-functionalized carbon nanotube; $NiFe_2O_4$/rGO- nickel ferrite/reduced graphene oxide; MIP-MWCNTs- molecularly imprinted polymer- multi-walled carbon nanotubes.

Table S7. Comparison table of MD determination.

Materials	**Linear range (μM)**	**Limit of detection (μM))**	**pH**	**Detection technique**	**Ref.**
Fe_3O_4/N/C@MWCNTs-2-600	1-725	0.19	7	DPV	11
Ag/Au-Nafion-coated GCE	100-1000	0.0587	7	DPV	12
ATO	0.1-104.3	0.011	8	DPV	13
C60-rGO-NF	0.5-34	0.035	7	SWV	14
Au NPs@PDDA/GH	0.4-656.4	0.097	7.0	LSV	15
NiMnO@pr-GO	0.1-234	0.090	7.0	DPV	16
Pt-nanospheres/ polyfurfural film	2.5-500	0.050	10	DPV	17
CdS QD@rGO	0.1-203.1	0.053	7.0	DPV	18
$CeVO_4$	0.02-75	0.0045	7.0	DPV	19
g-C_3N_4/MnO_2/ZnO	2-250	0.21	8.0	DPV	20
LFO/rGO	0.2-1221	0.048	7.0	DPV	21
$SmVO_4$	**0.1-161.0**	**0.0036**	**7.0**	**DPV**	**This work**

Fe_3O_4- iron oxide; Ag/Au-Nafion- silver/gold-nafion; ATO- silver titanate; C60-rGO-NF- fullerene-reduced graphene oxide-nafion; Au NPs@PDDA/GH- gold nanoparticle embedded poly(diallyldimethylammonium chloride)–graphene oxide hydrogels; NiMnO@pr-GO- nickel-manganous oxide@partially reduced graphene oxide; CdS QD@rGO- cadmium sulfide quantum dots@reduced graphene oxide; $CeVO_4$- cerium vanadate; g-C_3N_4/MnO_2/ZnO- graphitic carbon nitride/manganese dioxide/zinc oxide; LFO/rGO- lanthanum ferrite/ reduced graphene oxide

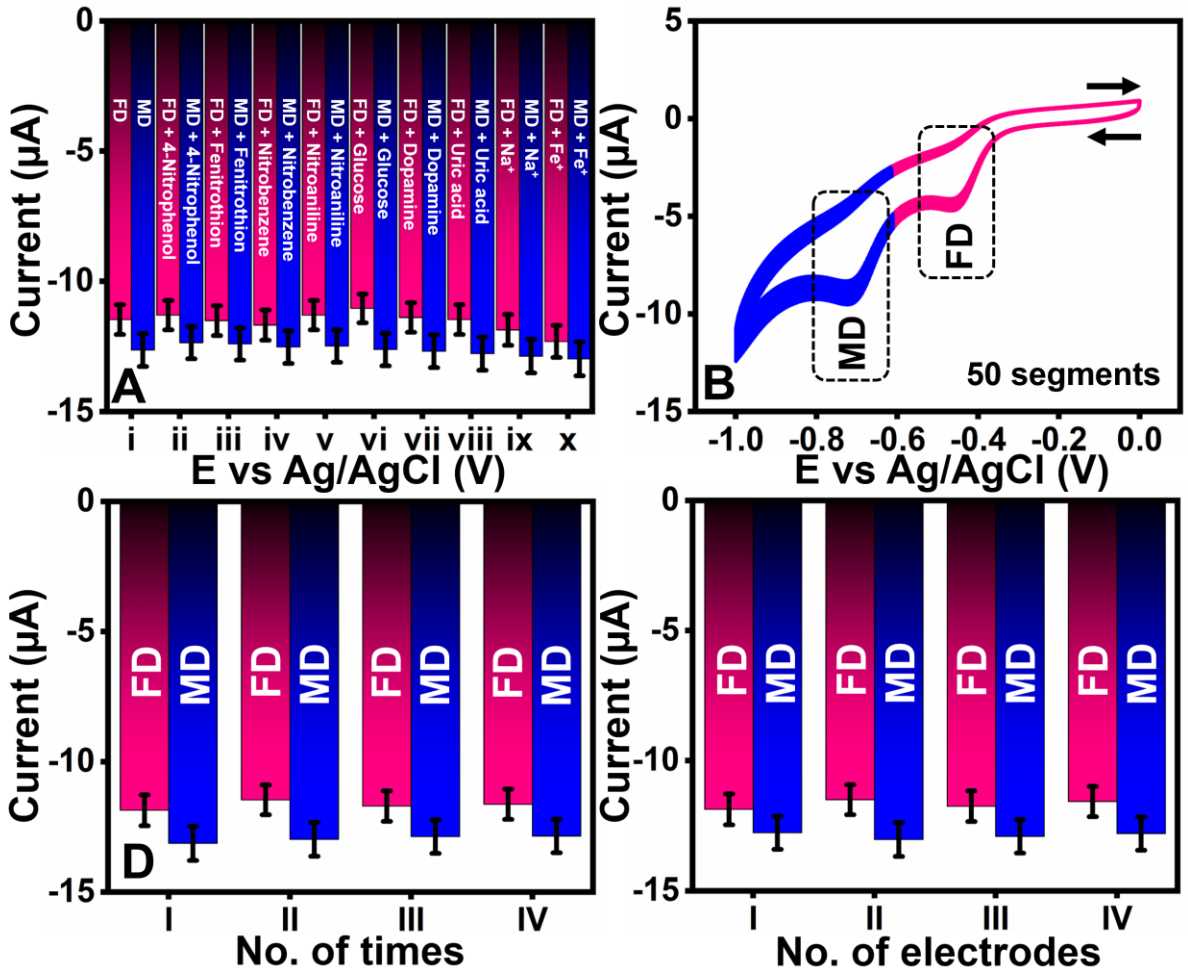

Figure S5. DPV results of SmV/GCE in FD & MD (A) with co-interfering compounds, (B) cyclic stability, (C) repeatability, (D) reproducibility.

Table S8. Determination of FD in Real-world samples at SmV/GCE

Sample	Added (μM)	Detected (μM)		Detection rate (%) (Mean ± RSD) (n = 3)
		DPV	HPLC	
BSA	0	–	–	–
	5	4.90	4.95	98.00 ± 0.20
	10	9.94	9.97	99.40 ± 0.015
	15	14.71	14.95	98.06 ± 0.019
Human urine	0	–	–	–
	5	4.85	4.98	97.00 ± 0.018
	10	9.93	9.99	99.30 ± 0.42
	15	14.80	14.92	98.66 ± 0.24
River water	0	–	–	–
	5	4.92	4.97	98.40 ± 0.33
	10	9.96	9.98	99.60 ± 0.012
	15	14.83	14.97	98.86 ± 0.025

Table S9. Determination of MD in Real-world samples at SmV/GCE

Sample	Added (μM)	Detected (μM)		Detection rate (%) (Mean ± RSD) (n = 3)
		DPV	HPLC	
BSA	0	–	–	–
	5	4.87	4.96	97.40 ± 0.23
	10	9.95	9.97	99.50 ± 0.012
	15	14.61	14.99	97.40 ± 0.015
Human urine	0	–	–	–
	5	4.96	4.98	99.20 ± 0.007
	10	9.90	9.98	99.00 ± 0.31
	15	14.75	14.99	98.33 ± 0.04
River water	0	–	–	–
	5	4.90	4.98	98.00 ± 0.093
	10	9.97	9.99	99.70 ± 0.022
	15	14.60	14.98	97.33 ± 0.011

Reference

1. Shahrokhian, S., Naderi, L. and Ghalkhani, M., 2016. Modified glassy carbon electrodes based on carbon nanostructures for ultrasensitive electrochemical determination of furazolidone. Materials Science and Engineering: C, 61, pp.842-850.

2. Fotouhi, L., Nemati, M. and Heravi, M.M., 2011. Electrochemistry and voltammetric determination of furazolidone with a multi-walled nanotube composite film-glassy carbon electrode. Journal of Applied Electrochemistry, 41, pp.137-142.

3. He, B.S. and Du, G.A., 2017. A simple and sensitive electrochemical detection of furazolidone based on an Au nanoparticle functionalized graphene-modified electrode. Analytical methods, 9(30), pp.4341-4348.

4. Balasubramanian, P., Annalakshmi, M., Chen, S.M. and Chen, T.W., 2019. Sonochemical synthesis of molybdenum oxide (MoO3) microspheres anchored graphitic carbon nitride (g-C3N4) ultrathin sheets for enhanced electrochemical sensing of Furazolidone. Ultrasonics Sonochemistry, 50, pp.96-104.

5. Kokulnathan, T., Wang, T.J., Thangapandian, M. and Alaswad, S.O., 2020. Synthesis and characterization of hexagonal boron nitride/halloysite nanotubes nanocomposite for electrochemical detection of furazolidone. Applied Clay Science, 187, p.105483.

6. Veerakumar, P., Sangili, A., Chen, S.M., Pandikumar, A. and Lin, K.C., 2020. Fabrication of platinum–rhenium nanoparticle-decorated porous carbons: voltammetric sensing of furazolidone. ACS sustainable chemistry & engineering, 8(9), pp.3591-3605.

7. Amalraj, A.J.J., Umesh, N.M. and Wang, S.F., 2020. Synthesis of core-shell-like structure SnS2-SnO2 integrated with graphene nanosheets for the electrochemical detection of furazolidone drug in furoxone tablet. Journal of Molecular Liquids, 313, p.113554.

8. Sun, Y., Waterhouse, G.I., Xu, L., Qiao, X. and Xu, Z., 2020. Three-dimensional electrochemical sensor with covalent organic framework decorated carbon nanotubes signal amplification for the detection of furazolidone. Sensors and Actuators B: Chemical, 321, p.128501.

9. Ensafi, A.A., Zandi-Atashbar, N., Gorgabi-Khorzoughi, M. and Rezaei, B., 2019. Nickel-ferrite oxide decorated on reduced graphene oxide, an efficient and selective electrochemical sensor for detection of furazolidone. IEEE Sensors Journal, 19(14), pp.5396-5403.

10. Rebelo, P., Pacheco, J.G., Voroshylova, I.V., Melo, A., Cordeiro, M.N.D. and Delerue-Matos, C., 2021. Rational development of molecular imprinted carbon paste electrode for Furazolidone detection: Theoretical and experimental approach. Sensors and Actuators B: Chemical, 329, p.129112

11. Yuan, S., Bo, X. and Guo, L., 2019. In-situ insertion of multi-walled carbon nanotubes in the Fe3O4/N/C composite derived from iron-based metal-organic frameworks as a catalyst for effective sensing acetaminophen and metronidazole. Talanta, 193, pp.100-109.

12. Khanfar, M.F., Al Absi, N., Abu-Nameh, E.S., Saket, M.M., Khorma, N., Al Daoud, R. and Alnuman, N., 2019. Ag/Au modified nafion coated glassy carbon electrode for the detection of metronidazole. International Journal of Electrochemical Science, 14(4), pp.3265-3280.

13. Vinothkumar, V., Abinaya, M., Chen, S.M., Sethupathi, V. and Muthuraj, V., 2021. Ultrasound assisted synthesis of silver titanate for the differential pulse voltammetric determination of antibiotic drug metronidazole. Physica E: Low-dimensional Systems and Nanostructures, 134, p.114865.

14. Materón, E.M., Wong, A., Freitas, T.A., Faria, R.C. and Oliveira Jr, O.N., 2021. A sensitive electrochemical detection of metronidazole in synthetic serum and urine samples using low-

cost screen-printed electrodes modified with reduced graphene oxide and C60. Journal of Pharmaceutical Analysis, 11(5), pp.646-652.

15. Veerakumar, P., Sangili, A., Chen, S.M. and Lin, K.C., 2020. Ultrafine gold nanoparticle embedded poly (diallyldimethylammonium chloride)–graphene oxide hydrogels for voltammetric determination of an antimicrobial drug (metronidazole). Journal of Materials Chemistry C, 8(22), pp.7575-7590.

16. Vivekanandan, A.K., Subash, V., Chen, S.M. and Chen, S.H., 2020. Sonochemical synthesis of nickel-manganous oxide nanocrumbs decorated partially reduced graphene oxide for efficient electrochemical reduction of metronidazole. Ultrasonics Sonochemistry, 68, p.105176.

17. Huang, J., Shen, X., Wang, R., Zeng, Q. and Wang, L., 2017. A highly sensitive metronidazole sensor based on a Pt nanospheres/polyfurfural film modified electrode. RSC advances, 7(1), pp.535-542.

18. Gopi, P.K., Kesavan, G., Chen, S.M. and Ravikumar, C.H., 2021. Cadmium sulfide quantum dots anchored on reduced graphene oxide for the electrochemical detection of metronidazole. New Journal of Chemistry, 45(6), pp.3022-3033.

19. Radha, A. and Wang, S.F., 2023. Insight into lanthanides REVO 4 (RE= Ce, Pr, Nd): a comparative study on RE-site variants in the electrochemical detection of metronidazole in environmental samples. Environmental Science: Nano, 10(11), pp.3122-3135.

20. Zhang, S., Yu, S., Wang, X., Zhang, Y., Yue, Z., Li, C. and Ma, Y., 2024. A novel electrochemical sensor for the detection of metronidazole in honey using the g-C3N4/MnO2/ZnO modified electrode. Journal of Food Composition and Analysis, 127, p.105992.

21. Pandiyan, R., Vinothkumar, V., Chen, S.M., Sangili, A. and Kim, T.H., 2023. Integrated LaFeO3/rGO nanocomposite for the sensitive electrochemical detection of antibiotic drug metronidazole in urine and milk samples. Applied Surface Science, 635, p.157672.